

Raman Mapping: A local probe for core and interface of Si nanocrystals in Si-SiO₂ Nanocomposite

Ekta Rani¹, Alka A Ingale¹, A Chaturvedi², C Kamal³, M P Joshi², Aparna Chakrabarti³, Arup Banerjee⁴ and L M Kukreja²

¹Laser Physics Applications Section, Raja Ramanna Centre For advanced Technology, Indore-452013, INDIA

²Laser Material Processing Division, Raja Ramanna Centre For advanced Technology, Indore-452013, INDIA

³Indus Synchrotrons Utilization Division, Raja Ramanna Centre For advanced Technology, Indore-452013, INDIA

⁴BARC Training School at RRCAT, Raja Ramanna Centre For advanced Technology, Indore-452013, INDIA

E-mail: alka@rrcat.gov.in

Abstract. Raman spectroscopy/mapping is used to investigate Si-SiO₂ multilayer nanocomposite grown using pulsed laser deposition. The Raman mapping of six films with Si deposition time in the range 45 – 210 s, shows primarily three different regions of Si phonon frequencies in Si nanocrystals. The lowest frequency region ~ 495 - 510 cm⁻¹ and highest frequency region ~ 515 - 519 cm⁻¹ are attributed to have originated from Si-SiO₂ interface and core of Si nanocrystals, respectively (Fig. 1). The consistent picture of this understanding is developed using Raman spectroscopy monitored laser heating and cooling experiment at the site of a desired frequency chosen with the help of Raman mapping. The same can be extended to explain variation observed in Si phonon frequencies of Si-SiO₂ nanocomposites reported in the literature. In order to support our experimental results, we also carry out Raman spectra calculations for Si₄₁ cluster with oxygen termination by employing *ab initio* density functional theory and time-dependent density functional theory based calculations. From our calculations, the frequency of phonon corresponding to the surface Si atoms is found to be at 512 cm⁻¹, which can be considered

analogous to the observed phonon frequencies in the range $495 - 510 \text{ cm}^{-1}$ originating from the Si-SiO₂ interface.

PACS: 72.80.Tm, 74.25.nd, 78.67.Bf and 74.25.Kc

Keywords: Nanocomposite, Raman spectroscopy, Si nanocrystals, Si-SiO₂ interface.

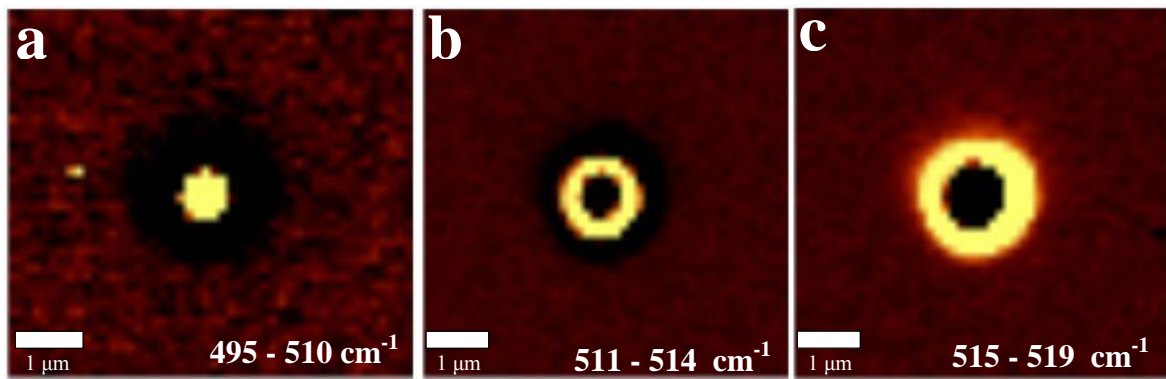


Fig. 1. Representative Raman image of sample E1 generated using phonon frequencies in the range a) $495 - 510 \text{ cm}^{-1}$, b) $511 - 514 \text{ cm}^{-1}$ and c) $515 - 519 \text{ cm}^{-1}$.

1. Introduction

Low dimensional semiconductor nanostructures have attracted great deal of attention in the last two decades because of their fundamental scientific interest, application in optoelectronic devices¹, and solar cells². Properties exhibited by nanocrystals (NCs) are size dependent due to quantum confinement effect and/or increase in surface to volume ratio. Among the semiconductor NCs, silicon nanocrystals (Si NCs) embedded in an insulating matrix, have been extensively studied because of their applications in solar cells and photonics. It has been found that an important factor determining the properties of Si NCs is the property of the insulating matrix in which the NCs are embedded³. Different types of insulating materials which have been used as matrix for Si NCs are SiO₂, Al₂O₃, Si₃N₄, and SiC.³⁻⁶ Out of these, especially SiO₂ matrix has been used to embed Si NCs to grow multilayer structure since multilayer structure can overcome the Shockley-Queisser limit of 30%. It has been reported that Si based tandem cell has theoretical efficiency of 60%.⁷ Raman mapping/spectroscopy is an ideal technique to study nanocomposites, as it gives information about local bonding environment, which may change within a nanocomposite. Noninvasive nature of Raman spectroscopy makes it more suitable local probe for understanding the nature and growth mechanism of the nanocomposite. Si (NCs or bulk) is one of the most studied materials using Raman spectroscopy, nevertheless repeatability and corroboration to other properties with Raman spectra has been difficult for different forms of Si (porous Si) or Si in different environment. Various techniques which have been used to grow Si NCs in matrix (especially SiO₂) are ion implantation,⁸⁻¹⁵ magnetron sputtering,¹⁶⁻²⁰ cluster beam deposition,²¹⁻²³ electron gun evaporation,²⁴⁻²⁵ plasma enhanced chemical vapor deposition,^{6, 26-29} gas evaporation,³⁰ co-sputtering,³¹ laser etching^{32, 33} and pulsed laser deposition (PLD)³⁴⁻³⁷. It is found that irrespective of the growth technique used for Si-SiO₂ nanocomposite,

variation in Si phonon frequency (in the range 495 - 519 cm^{-1}) has been reported in the literature. There have been few attempts to consolidate the findings^{9, 22, 25, 27} however, the variation of Si phonon frequency observed in these nanocomposites cannot be completely explained using presently proposed models.^{8, 22, 25, 38} In most of the techniques stated above, the growth is started with amorphous matrix of SiO_x and subsequent high temperature annealing leads to the formation of the nanocomposite of Si NCs in SiO_2 matrix. It is interesting to note that in PLD, however, alternate multilayer of Si NCs and SiO_2 are grown to form Si- SiO_2 nanocomposite and hence we wanted to check if we also find similar variation in Si phonon frequency under this growth condition. We also observe similar Si phonon peak variation of Raman data on Si- SiO_2 nanocomposite films grown using PLD.³⁹

In this paper, we have made an attempt to understand the origin of variation found in the Si-phonon peak frequency in Si- SiO_2 nanocomposites and provide more general and satisfactory explanation for the same. Since, we find lot of spatial variation in the Raman spectra of these Si- SiO_2 nanocomposites, Raman mapping is used to investigate the same. In order to understand the origin of this variation, we carry out laser heating & cooling (LHC) experiment on desired frequency. This variation of the Si phonon peak position and line shape obtained in these nanocomposites has been attributed to the local variation of Si NCs/ SiO_2 interface in the SiO_2 matrix and size of the Si NC. In the process of this analysis, consolidation and understanding of the data available in the literature is also achieved. Further, to gain more insight we carry out *ab initio* density functional theory (DFT) and time-dependent density functional theory (TDDFT) based calculations of Raman spectra of optimized Si cluster (Si_{41}) terminated by O and H atoms.

The present paper is organized in the following manner. In section 2, Raman spectroscopy and mapping experiments are described. Section 3 and 4 are devoted to Raman

spectroscopy and Raman mapping results showing spatial variation in Si phonon frequency. In section 5, we discuss these results to construct a consistent picture based on our understanding that low frequencies (in the range 495 - 510 cm^{-1}) and high frequencies (in the range 515 – 519 cm^{-1}) Si phonons originate from different parts of a Si nanocrystal in Si-SiO₂ nanocomposite. In the same section, the results of calculated Raman spectra on Si₄₁ cluster are also presented. The understanding developed from LHC experiment and its corroboration with the calculated Raman spectra is summarized in the conclusion.

2. Experimental

Si-SiO₂ multilayer nanocomposites are grown using PLD. Silicon NCs of variable mean sizes are grown by varying the deposition time of Si from 45 to 210 s. These multilayer (15) films are subsequently annealed at 800 °C in the PLD chamber in the nitrogen ambience.³⁹ We have studied 6 samples with varying Si deposition time and these samples are designated as 1) E1 (45s), 2) E2 (90 s), 3) E3 (120 s), 4) E4 (150 s), 5) E5 (180 s), and 6) E6 (210 s) with numbers appearing in the parenthesis denotes the deposition time in seconds. Micro-Raman spectroscopy measurements are performed at room temperature using NSOM-SPM integrated Raman system set up, Witec (Germany). The samples grown Si-SiO₂ nanocomposites are excited with 442 nm wavelength of He-Cd laser using a 50x microscope objective lens of numerical aperture 0.55 with spatial resolution of ~ 1.2 μm . Raman spectrum is collected in the back scattering geometry and dispersed using single spectrometer of half meter focal length. Notch filter is used for stray light rejection. Data is collected using air cooled charged coupled device (CCD) detector.

3. Raman spectroscopy

In our previous study of Raman spectroscopy of this nanocomposite,³⁹ we have observed the following: i) Sizes obtained from line shape fitting for these multilayer nanocomposites are much larger than measured by transmission electron microscopy (TEM) for a monolayer Si-SiO₂ film and ii) The observed red shift is not in agreement with the red shift calculated using phonon confinement model (PCM) given by Campbell and Fauchet.⁴⁰

When measured at spatially different positions, Raman spectroscopic measurements of Si-SiO₂ nanocomposite/films further show variation in the Si phonon frequency from 495 to 519 cm⁻¹ in all the samples (E1-E6). It is well known that Raman spectra of Si NCs show asymmetric phonon line shape and red shift in phonon frequency due to phonon confinement effect accounted by PCM noted above.^{40, 41} It is found that primarily PCM has been used to explain similar Raman spectroscopy results reported in Si NCs grown using various techniques.^{8-9, 31 & 42-44} Further, in the literature, it is noted that PCM alone is inadequate to give correct red shift and line shape fitting simultaneously for Si NCs.^{21-22, 25, 33, 44-46} Several groups have addressed this discrepancy and different solutions have been proposed to obtain correct redshift along with correct line shape fitting using PCM model. In the following, various solutions are discussed along with reference to the results reported in the literature:

i) Bond Polarizability (BPL) model: BPL model⁴⁵ has been used for calculating sizes (<50 Å) of Si NCs from the observed red shift^{22, 24-25, 47} whereas; PCM is used for calculating the line shape of the same. Wei-Long et al.²⁴ and Stenger et al.²⁵ have reported the agreement between size calculated using BPL model and size observed by TEM for phonon frequencies in the range 514 - 518 cm⁻¹ for Si NCs in SiO₂ matrix, but no special information regarding line shape fitting is provided. However, Gupta et al. have shown that even BPL model is unable to give accurate results below the Si phonon frequency ~ 512 cm⁻¹.⁴⁸ This suggests that BPL model does not give

correct results for low phonon frequencies. In our case, we find that the sizes calculated from BPL model (Table-1) are not in agreement with the TEM measurements.³⁹ This suggests that the large red shift in the Si phonon frequency observed by us may not be solely due to confinement (Si NCs), but can have some different origin.

Samples	Phonon frequency (cm ⁻¹)	Sizes calculated using BPL model (Å)	Sizes observed from TEM measurements (Å)
E1 (45s)	502	10.5	1.4
E2 (90s)	514	26.7	2.9
E4 (150s)	516	31	4.0

Table 1: Comparison of sizes calculated using BPL model for frequencies noted in the earlier paper and sizes measured from TEM measurements.

ii) Modified PCM (inclusive of size distribution): In order to reproduce correct line shape and frequency of the observed Si phonon simultaneously, size distribution of Si NCs has been accounted for by some authors.^{8, 38} Crowe et al.⁸ and Mavi et al.³⁸ have reported that PCM gives good results after including log normal and Gaussian distribution respectively for phonon frequencies in the range 516 - 522 cm⁻¹. In our case, red shift observed for phonon frequencies (495 - 514 cm⁻¹) cannot be obtained even after including the size distribution.

iii) Laser heating: Literature has several reports showing red shift in Si phonon peak due to laser heating even at small laser power density (PD) ~ 5 - 10 kW/cm² for visible region.^{24, 38, 49-50} It has been reported that there is an induced red shift of ~ 1 cm⁻¹ for Si NCs embedded in SiO₂ grown on Si substrate at laser PD: 5 kW/cm²²⁴ whereas, for isolated Si NCs grown on sapphire

substrate using continuous wave laser annealing of amorphous Si: H films, induced red shift is $\sim 2 \text{ cm}^{-1}$ at laser PD $\sim 5 \text{ kW/cm}^2$.³⁸ In our case we have used laser PD $\sim 2\text{-}5 \text{ kW/cm}^2$. It is important to note that laser heating will depend on laser PD as well as matrix used for Si NCs, as heat dissipation will be function of matrix material and structure of the nanocomposite. Therefore, red shift of Si phonon peak in our case due to laser heating can be safely taken to be in between the above two cases and hence, we believe that the observed large red shift in our case is not due to laser heating.

We have investigated this variation of Si phonon frequency in further detail using Raman mapping.

4. Raman mapping: Si phonon peak variation

Many sets of Raman mapping (acquisition time 1 s) are performed on each of the six samples. Since, Raman spectra show phonon frequencies in the range $495 - 519 \text{ cm}^{-1}$ for all the samples, hence Raman images are generated using phonon frequencies in the range $490 - 525 \text{ cm}^{-1}$. Representative Raman image for sample E1 is shown in Fig. 1(a) and Fig. 1(b) shows corresponding Raman spectra for the marked positions in Fig. 1(a). Raman image (Fig. 1) shows clustering of Si NCs in this nanocomposite. This cluster formation is being further investigated using Raman mapping and AFM and details will be published elsewhere.⁵¹ Fig. 1(b) shows that there is variation in the line shape of Si phonon as it goes from 495 to 519 cm^{-1} and can be separated in three different regions as follows, i) $495 - 510 \text{ cm}^{-1}$ (LF): line shape of Si phonon in this range can be well fitted using Lorentzian line shape (Fig. 1(b)), ii) $515 - 519 \text{ cm}^{-1}$ (HF): asymmetric line shape (A1) for this range phonons can be well fitted using PCM (Fig. 1(b)) and iii) $510 - 514 \text{ cm}^{-1}$ (IF): asymmetric line shapes (A2) of phonons in this range cannot be fitted with either single Lorentzian peak or using PCM. By selecting LF, IF and HF range of

frequencies, separate Raman images of the selected area Raman mapping are created. Representative Raman images for LF, IF and HF phonons for the sample E1 are shown in Fig. 1(c)-1(e).

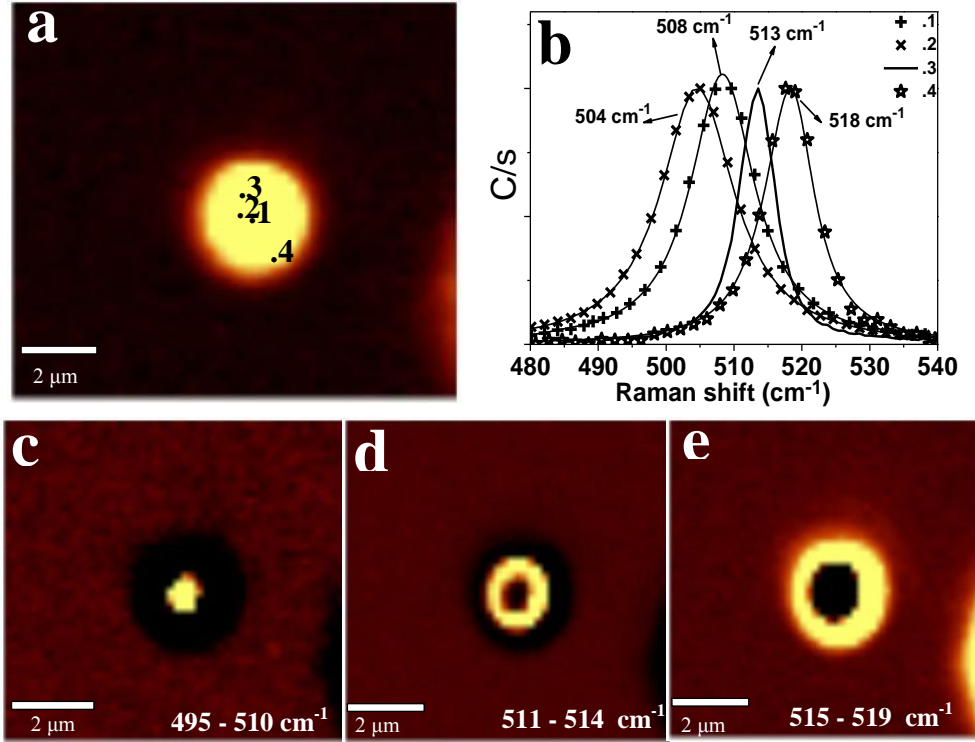


Fig. 1. a) Representative Raman image of sample E1 generated using frequency in the range $495 - 525 \text{ cm}^{-1}$ and (b) Corresponding Raman spectra on positions as marked in Raman image (a) showing Lorentzian line shape for phonon frequencies ~ 504 and 508 cm^{-1} , PCM fit asymmetric line shape (A1) for phonon frequency $\sim 518 \text{ cm}^{-1}$ and asymmetric line shape (A2) for phonon frequency $\sim 513 \text{ cm}^{-1}$. Raman image generated using phonon frequency c) $\sim 495 - 510 \text{ cm}^{-1}$, d) $511 - 514 \text{ cm}^{-1}$, e) $\sim 515 - 519 \text{ cm}^{-1}$.

While performing Raman spectroscopic measurements in all the samples, we have also observed simultaneous occurrence of LF and HF phonons $\sim 501 \text{ cm}^{-1}$ and $\sim 517 \text{ cm}^{-1}$ respectively, at some spatial positions. Similar kind of observation is reported earlier by Faraci et al.²² in Si-SiO₂ nanocomposite grown using cluster beam deposition. Faraci et al. have suggested that lower frequencies may be due to Si aggregates having a thin SiO_x (with $x = 1 - 2$) interface

for Si NCs in SiO₂ matrix.²² Considering the above, we investigate the following three different possibilities for occurrence of these two peaks:

- i) If the two peaks are originating from two different sizes then a) the intensity for the peak with higher frequency is expected to be more compared to that of peak with lower frequency, as there will be larger contribution to the Raman scattering from larger size particles. Unless, there is evidence that number of smaller NCs is countering the volume ratio, this statement is valid. b) With the decrease in size, asymmetry of the Si phonon should increase, which is not observed by us and c) Laser heating/annealing may bring about coalescence of these Si NCs in SiO₂ leading to the increase in the average size of NCs.⁵²
- ii) If two peaks are originating from different local stress then laser heating/annealing can lead to relaxation of the residual stress, red shifting both the phonon frequencies.
- iii) If two peaks are originating from core and interface of Si NC then laser heating/annealing may lead to different behavior in case of two phonon frequencies.

To check all the above possibilities, we have performed Laser heating and cooling (LHC) experiment on four kinds of Si phonon peaks observed here as i) LF phonons, ii) IF phonons, iii) HF phonons and iv) Simultaneously observed LF and HF phonons.

4.1. Raman spectroscopy monitored Laser heating and cooling (LHC) experiment: While performing this experiment, no mechanical movement is involved. Laser excitation used is 441.6 nm and laser power is kept low (PD ~ 5 kW/cm²). Steps of LHC experiment are described below:

1. The desired peak frequency is located using Raman mapping for doing LHC experiment on the said frequency ranges.

2. Laser heating and cooling steps:

1st step; 2nd step: *laser on for 16 mins*; 3rd step: *Laser shutter off for 40 mins*; 4th step: *Again laser on for 16 mins*; 5th step: *Laser shutter off for 3 hrs*.

At the end of each step Raman spectrum is recorded with acquisition time 3 s. LHC experiment is performed on each sample for at least 2-3 frequencies in each of the three phonon ranges (LF, IF, HF) noted earlier. The effect of LHC experiment on LF, IF and HF phonons is found to be different. It is important to note that observations for LF and HF phonons during LHC are same irrespective of their simultaneous or separate occurrence in the Raman spectra. The results are summarized in the following.

i) LF phonons ($495 - 510 \text{ cm}^{-1}$): In all the measurements performed in this frequency range, the behavior of peak frequencies is similar i.e. it blue shifts during LHC. Representative Raman spectra for phonon frequency $\sim 499 \text{ cm}^{-1}$ during LHC experiment is shown in Fig. 2(b). This peak shows continuous blue shift of $\sim 10 \text{ cm}^{-1}$. Further, crystalline order has increased on laser heating (annealing) as FWHM has decreased by $\sim 4.5 \text{ cm}^{-1}$ during the experiment. Raman line shape of these LF phonons is Lorentzian.

ii) HF phonons ($515 - 519 \text{ cm}^{-1}$): In all the measurements performed in this frequency range, phonons show similar behavior i.e. it does not change during LHC. Representative Raman spectra for phonon frequency $\sim 516 \text{ cm}^{-1}$ during LHC experiment is shown in Fig. 2(c). This peak does not change during the entire experiment. Line shape of these phonon is asymmetric, which can be well fitted using PCM. The size obtained from PCM fit is $\sim 90 - 100 \text{ \AA}$.

iii) Simultaneously observed LF and HF phonons $\sim 501 \text{ cm}^{-1}$ and $\sim 517 \text{ cm}^{-1}$ respectively: The two peaks Raman spectra (Fig. 2(a)) are approximated as two Lorentzians for convenience of noting the variation in the frequency. Out of the two peaks LF phonon shows total blue shift by $\sim 4 \text{ cm}^{-1}$, whereas HF phonon does not show any significant change.

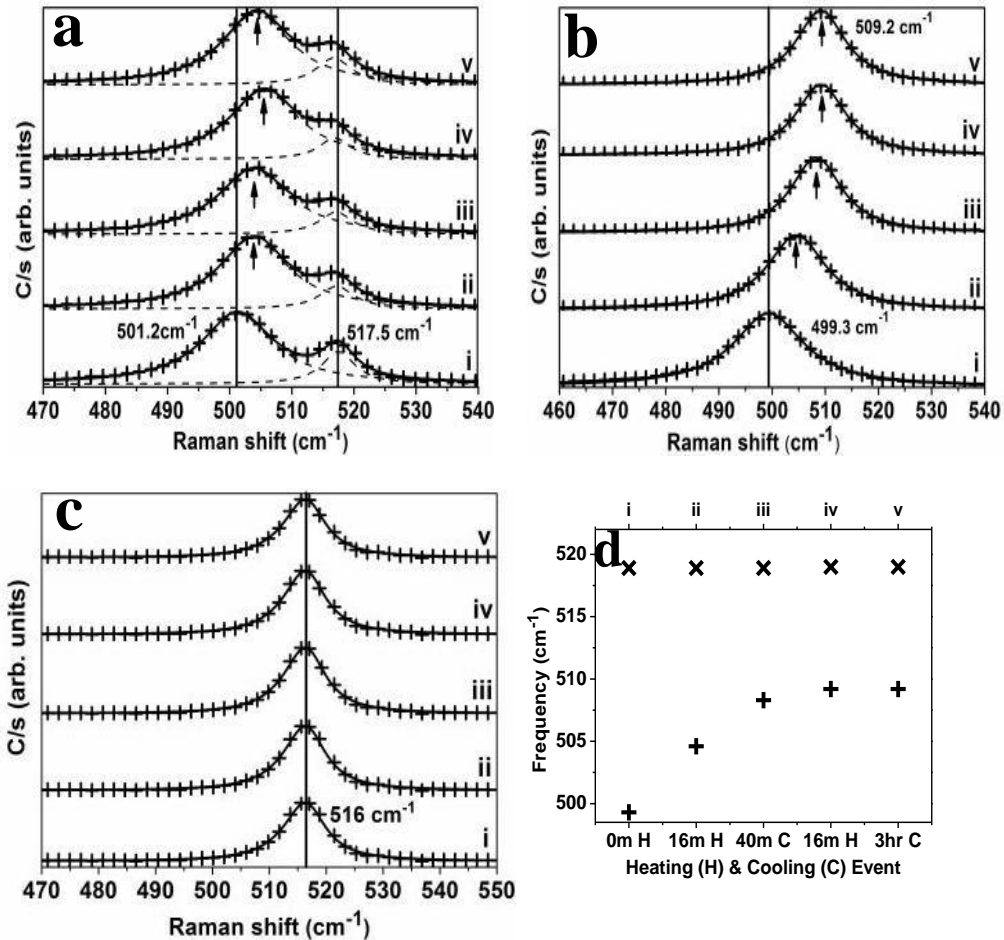


Fig. 2. Representative Raman spectra showing change for a) two resolvable phonon frequencies occurring simultaneously ~ 501 and 517 cm^{-1} , b) phonon frequency $\sim 499 \text{ cm}^{-1}$, c) phonon frequency $\sim 516 \text{ cm}^{-1}$ occurring separately during 5 steps of LHC experiment as (i) 0 min heating, (ii) 16 min heating, (iii) 40 min cooling, (iv) again 16 min heating and (v) 3hr cooling. Raw data points are shown by (+) and the solid line is the line shape fit to the spectra as noted in the text and d) Change in LF and HF phonon during LHC process. Symbols (+) and (x) show phonon frequency $\sim 499 \text{ cm}^{-1}$ and 517 cm^{-1} .

iv) IF phonons: Modes in this frequency range follows LF behavior during LHC experiment, however, shows some differences with respect to LF phonons. Details will be published elsewhere.⁵³

The variation of peak frequency obtained in 5 steps of heating and cooling experiment for different range peak frequencies is summarized in Fig. 2(d).

5. Discussion

Considering that LF and HF phonons originate from different size Si NCs; one would expect LHC will bring about coalescence of these NCs increasing the average size of NCs, which may lead to blue shift in phonon frequency in both the cases. However, we have observed blue shift only for LF phonons (frequency range 495 - 510 cm^{-1}). Further, the fact that line shape of LF phonons is Lorentzian and not asymmetric refutes that it can have origin as smaller size Si NCs.

Considering the second possibility of LF and HF phonons occurring due to different local stress, one would expect that LHC should lead to either relaxation of the residual stress or increase in stress, simultaneously for both the phonon peaks. However, the heating/annealing effect for low and high frequency phonons is quite different indicating that they might have different origins.

A third possibility which can be considered is that the LF and HF phonon are originating from different parts of Si NCs. We attribute the origin of LF phonons to the interface of Si-SiO₂ and HF phonons to the core of Si NCs, respectively. The manifold reasons and consistencies in the observations noted earlier to reach this interpretation are listed in the following:

1) There are some theoretical predictions and experimental reports regarding the presence of different Si sub oxides (Si^{1+} , Si^{2+} , Si^{3+}) at the surface of Si NC in Si-SiO₂.^{54, 55, 56} Molecular dynamics simulation shows that oxidation leads to stretching of Si-Si bonds around the interface only.⁵⁷ Further, vibrational density of states (VDOS) calculations show that at the surface of nanocrystals, phonon frequencies up to 494 cm⁻¹ can be observed.⁵⁸ Furthermore, the presence of different types of defects has been predicted at the interface in the presence of oxygen, which increases with the increase in oxidation.^{55, 59} Consistent with this we attribute the LF phonons due to stretching mode of Si-Si bonds at the Si-SiO₂ interface. The phonon frequency range from 495 to 510 cm⁻¹ can be attributed to variation in local SiO_x environment seen by Si-Si bonds. This will also lead to a Lorentzian line shape of Si-Si stretching vibration with appropriate width depending on SiO_x environment as observed by us. Therefore, we attribute LF phonons in the range 495 - 510 cm⁻¹, as originating from the interface of small Si NCs in Si-SiO₂.

The blue shift in LF phonons (Fig. 2(d)) with betterment in crystalline order during LHC experiment can be understood in terms of more crystalline Si-Si bonding environment leading to more ordered Si-SiO₂ interface.

2) The asymmetric line shape of HF phonons observed in the range 515 - 519 cm⁻¹ is attributed to the core of Si NCs as the asymmetry can be fitted satisfactorily by PCM fit which does not show any change in frequency, width & line shape during LHC experiment.

This further suggests that the changes observed for LF phonons during LHC may be due to only surface/interface reconstruction of smaller Si NCs with laser heating in Si-SiO₂ nanocomposite.⁶⁰

5.1. Understanding variation in blue shift of Si phonons originating at the interface (LF phonons) during LHC:

Variation in blue shift of various LF phonons in the range $495 - 510 \text{ cm}^{-1}$ is plotted in Fig. 3(a) during 5 steps of LHC. It is interesting to note that primarily there are two types of patterns in change of frequencies during LHC experiment. i) In one pattern, last three steps show no further change in frequency i.e. irreversibility during heating and cooling process and ii) In another pattern, last three steps show increase and decrease of frequencies i.e. reversibility during heating and cooling process. These patterns can be understood in terms of elastic/plastic behavior of the matrix i.e. the frequency of Si phonon saturates when interface is not changing due to heating/cooling as discussed in the following.

Elastic/plastic transition for Si NC⁶¹ and amorphous SiO₂⁶² has been studied separately. In our case, elastic/plastic transition of amorphous SiO₂ is the relevant phenomenon. It has been reported that elastic to plastic transition occurs at 2.5 GPa with the rearrangement of atoms i.e. without the formation of dislocations and is an irreversible effect.⁶² Creation of such a pressure in Si-SiO₂ nanocomposite on heating/cooling experiment is a possibility, as it requires only the rearrangement of atoms at the interface. Thus SiO₂ matrix plays an important role in freezing the frequency of LF phonons on further heating or cooling, when it has already reached the plastic transition. On the other hand, the red shift occurs in 5th step of LHC i.e. after 3 hrs cooling time, when SiO₂ near the Si NC surface is still in the elastic region. It may be interesting to independently explore this phenomenon further.

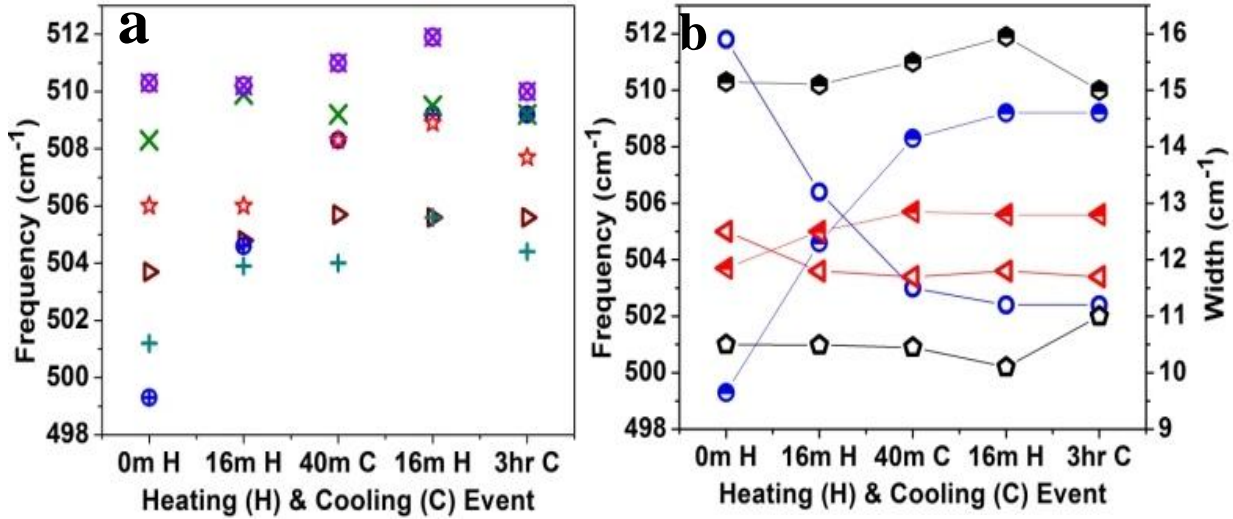


Fig. 3. a) Change in phonon frequency during LHC experiment for LF phonons in the range ~ 495 to 510 cm^{-1} and b) Change in phonon frequency and corresponding FWHM during LHC experiment for LF phonons. Half filled symbols show frequency and open symbols show corresponding FWHM.

5.2. Measurement of local temperature: Stoke/anti-Stokes Raman

There is one more important point to note here that the variation of phonon frequency and FWHM are mirror images of each other (Fig. 3(b)) during LHC experiment. For lower phonon frequency, FWHM is higher and one can also see that blue shift in phonon frequency is always accompanied with betterment in crystalline order of the interface for all the frequencies plotted here. This behavior of the phonon peak and corresponding FWHM is similar as due to change in the temperature of a crystalline material. For bulk and nanocrystalline Si, temperature dependent Raman studies show that red shift of the optical phonon mode by $\sim 10 \text{ cm}^{-1}$ and $\sim 15 \text{ cm}^{-1}$ respectively, for temperature rise from 300 to 800K.^{63, 64} Thus to obtain the local temperature during LHC experiment, we have performed Stokes/anti-Stokes Raman measurements. Local temperature calculated using intensity ratio of Stokes to anti-Stokes (I_S/I_{AS})⁶³ of HF phonon is found to be the room temperature (300K). This is consistent with the fact that no change in HF

phonon is observed. However, local temperature calculated using LF phonon (interface frequencies) is found to be in the range of ~550-700K (at spatially different positions). Further, during LHC experiment, LF phonons show change in the local temperature as shown in Fig. 4. Moreover, continuous blue shift doesn't show a continuous decrease in temperature indicating that there exists no correlation between frequency shift of the phonon and the temperature obtained from Stoke/anti-Stoke Raman measurements. It is important to note that the two different local temperatures at a site, obtained using two different phonons is difficult to explain. The question is, if we are actually having core and interface of Si NC at two different temperatures i.e. core at room temperature (300K) and interface at 600K during the LHC experiment. As we are heating the Si NC, heat is flowing from core to surface and it is getting trapped there because of presence of insulating SiO₂ matrix and this may increase the temperature at the surface. However, after 16 mins (after 2nd step in Fig. 4) of heating we observe a decrease in measured temperature, suggesting that there are inconsistencies in this interpretation. The second plausible explanation is that the local temperature calculated from I_S/I_{AS} data using interface/surface phonon (LF phonons) may not be correct. This can happen, if excitation source is close to one of the real energy levels of the system, leading to resonance Raman scattering. Resonance Raman scattering is indeed observed for LF phonons and detailed study of the same is in progress and will be published separately.⁵³ Different local temperatures calculated using I_S/I_{AS} of LF and HF phonons further confirms that both LF and HF phonons have different origin.

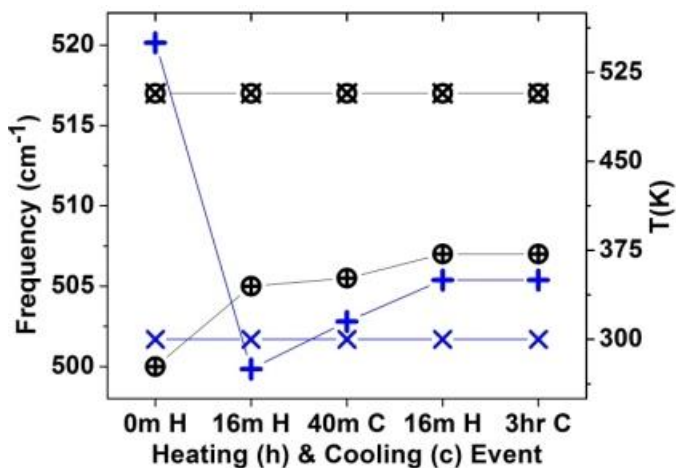


Fig. 4. Change in frequency and calculated local temperature during LHC experiment for LF and HF phonons. Symbols (+) and (×) in circle show LF and HF phonon and symbols (+) and (×) show corresponding local temperature.

Furthermore, to gain more insight we carry out *ab initio* DFT and TDDFT based calculations of Raman spectra of optimized Si cluster (Si_{41}) terminated by O and H atoms as discussed in the next subsection.

5.3. Calculation of Raman spectra of Si cluster (Si_{41}) with different terminations:

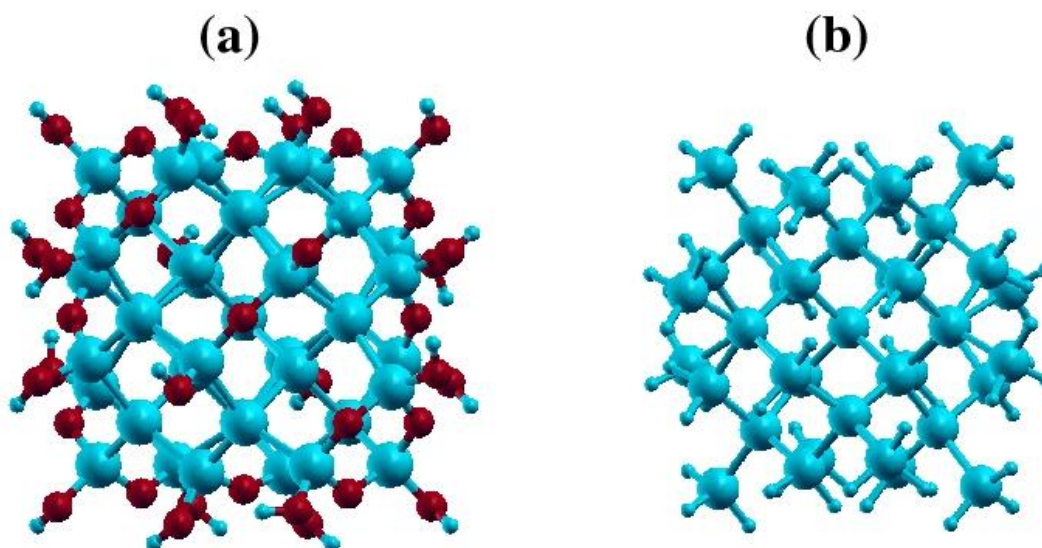


Fig. 5. Ball and stick model for the optimized geometric structures of Si_{41} cluster with (a) oxygen ($\text{Si}_{41}\text{O}_{42}\text{H}_{24}$) and (b) hydrogen atoms ($\text{Si}_{41}\text{H}_{60}$) terminations which are obtained by DFT based electronic structure calculation with PBE XC functional and TZ2P basis set. The balls with colors cyan (large), red (medium) and cyan (small) represent Si, O and H atoms respectively.

In order to support our experimental results as well as to gain microscopic understanding, we perform density functional theory⁶⁵ based electronic structure calculations for a medium size silicon cluster (Si_{41}), with bulk-like tetrahedral coordination, using Amsterdam Density Functional (ADF) code.⁶⁶ We consider two possible terminations for silicon atoms present at the surface of the cluster, namely (a) oxygen and (b) hydrogen atoms, in order to avoid the dangling bonds. The former termination is used to mimic the Si cluster/ SiO_2 interface. The calculations of ground state properties have been carried out by using triple- ξ Slater-type orbital (STO) basis set with two added polarization functions (TZ2P basis set of ADF basis set library)⁶⁶ along with generalized gradient approximation (given by Perdew-Burke-Ernzerhof (PBE)⁶⁷) exchange-correlation (XC) functional. The geometric structures of the cluster with the two above mentioned terminations, and with bulk-like initial positions, are fully relaxed using the BFGS technique until the norm of the energy gradient and energy attain values less than 10^{-4} au and 10^{-6} au respectively.

The fully optimized geometric structures of Si_{41} cluster with (a) oxygen ($\text{Si}_{41}\text{O}_{42}\text{H}_{24}$) and (b) hydrogen atoms ($\text{Si}_{41}\text{H}_{60}$) terminations are shown in Fig. 5. The results of our detailed geometric analysis are summarized in Table 2. We observe from this table that the mean values for Si-Si bond lengths (2.38 in $\text{Si}_{41}\text{O}_{42}\text{H}_{24}$ and 2.37 Å in $\text{Si}_{41}\text{H}_{60}$) are slightly higher than its corresponding value of 2.34 Å in bulk silicon. This indicates that the interaction between Si atoms in the cluster is little weaker than that in the bulk form. The maximum variation in the value of bond length, with respect to its bulk value is 0.07 Å. The trend of increase in the mean values for these angles is given in 4th - 6th columns of Table 2. The standard deviations (SD) for both the bond lengths and bond angles are also given in Table 2. The calculated mean values (109.23 and 107.64° for $\text{Si}_{41}\text{O}_{42}\text{H}_{24}$ and $\text{Si}_{41}\text{H}_{60}$ respectively) of bond angles in the core region

indicate that the local environment of Si atom in this region is bulk-like since these values are close to the corresponding bond angle (109.47°) between the Si atoms in bulk. However, we observe large modifications in the mean values of the bond angles between Si atoms as we go to the surface region. Our results show that there exist two different types of bond angles in the surface region: one value is much lower and another being higher than that of in the core region. In case of $\text{Si}_{41}\text{O}_{42}\text{H}_{24}$, we also find different types of bond angles between Si and O atoms in the surface region. Overall, our results of geometric analysis clearly indicate that the hybridization between Si atoms in the core region is nearly sp^3 -like and it is modified in to a mixture of sp^2 and sp^3 in the surface regions.

System	Bond length (Å)		Bond angle (°)					
	Si-Si	Si-O	Si-Si-Si (Core)	Si-Si-Si (Core/Surf.)	Si-Si-Si (Core/Surf.)	O-Si-O	Si-O-Si	Si-O-Si
$\text{Si}_{41}\text{O}_{42}\text{H}_{24}$								
Mean	2.38	1.66	109.23	100.23	117.10	107.79	126.32	147.18
SD	0.016	0.009	1.05	1.53	2.87	2.07	0.46	0.50
$\text{Si}_{41}\text{H}_{60}$								
Mean	2.37	1.504	107.64	103.06	117.40	107.78	-	-
SD	0.016	0.005	1.07	1.15	0.11	0.60	-	-

Table 2: The results for the bond lengths and bond angles of Si_{41} cluster with (a) oxygen ($\text{Si}_{41}\text{O}_{42}\text{H}_{24}$) and (b) hydrogen atoms ($\text{Si}_{41}\text{H}_{60}$) terminations obtained by DFT based electronic structure calculation with PBE XC functional and TZ2P basis set.

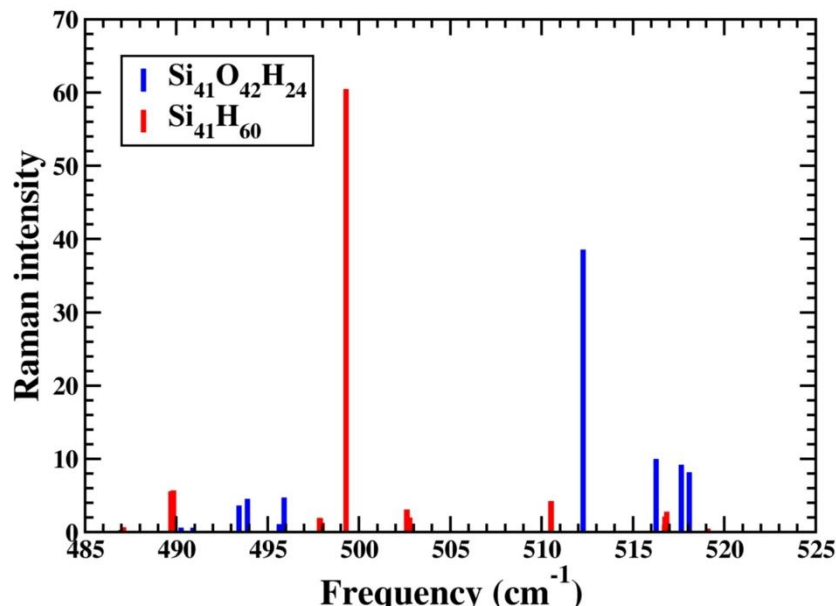


Fig. 6. Raman spectra of Si₄₁ cluster with (a) oxygen (Si₄₁O₄₂H₂₄) and (b) hydrogen (Si₄₁H₆₀) terminations obtained by employing DFT/TDDFT based response property calculation.

In order to gain more insight into the experimental results for Raman spectra discussed above we employ these optimized structures to perform calculations of Raman spectra. For this purpose we make use of linear response theory within TDDFT which is implemented in RESPONSE module of the ADF code.⁶⁶ The intensity of Raman spectra is calculated by estimating the first derivative of the polarizability with respect to normal coordinates. We use the same TZ2P basis set for the calculations of polarizability. It is well known that for performing calculations of response properties within TDDFT, it is required to use approximate forms for the XC potential at two different levels. At the first level, we use standard PBE XC potential for the calculation of ground-state Kohn-Sham orbitals and their energies. The second level of approximation is needed for XC kernel which determines the XC contribution to the screening of applied fields and for this we use the reasonably accurate adiabatic local density approximation (ALDA). The calculated Raman spectra of Si₄₁ cluster with (a) oxygen (Si₄₁O₄₂H₂₄) and (b) hydrogen atoms (Si₄₁H₆₀) terminations are presented in Fig. 6. It is observed from Fig. 6 that

there is a strong peak at 512 cm^{-1} in Raman spectra of oxygen terminated Si_{41} cluster. Similarly, we also observe a strong peak at 499 cm^{-1} in Raman spectra of hydrogen terminated Si_{41} cluster. It is important to note that the frequencies of these two strong peaks observed in Si_{41} cluster with oxygen and hydrogen atoms terminations are different and they are much lower than the corresponding Raman peak $\sim 521\text{ cm}^{-1}$ in bulk silicon. Furthermore, our detailed analysis shows that the normal modes of vibrations corresponding to these strong peaks contain motions of Si atoms lie on the surface of Si_{41} cluster. It is evident from our calculations that Si atoms at the surface of cluster and their local environments play an important role in determining Raman spectra. Thus, our calculated vibrational frequency ($\sim 512\text{ cm}^{-1}$) of the strong peak in oxygen terminated cluster can be analogous to the observed phonon frequencies ($495 - 510\text{ cm}^{-1}$) which are originating from the Si cluster / SiO_2 interface.

On the other hand, the calculated frequency of a strong peak in Raman spectra of hydrogen terminated cluster is much lower ($\sim 499\text{ cm}^{-1}$) than the corresponding frequencies in oxygen terminated cluster. These results are also consistent with the experimental data reported in the literature. In hydrogen passivated Si NCs (NCs Si: H), Raman spectra show phonon frequencies in the range $500 - 517\text{ cm}^{-1}$ with 514.5 nm as excitation laser.⁶⁸⁻⁷⁰ Whereas, Raman spectrum of NCs Si: H shows phonon frequencies $\sim 439, 462, 478, 486, 504\text{ cm}^{-1}$ with 496.5 nm as excitation laser.⁷¹ This suggests that in case of NCs Si: H, frequencies are found to be lower as compared to Si- SiO_2 nanocomposite. It is important to note here that observance of surface/interface phonons (LF) is laser excitation dependent.⁵³

6. Conclusion

We have studied PLD grown Si/SiO₂ multilayer nanocomposites with different Si layer thickness. Spatial variation of Si phonon frequencies in the range 495 - 519 cm⁻¹ has been investigated using Raman spectroscopy. To understand the origin of a Si- phonon frequency, Raman spectroscopy monitored local laser heating and cooling experiment is devised on the desired frequency. On the basis of line shape variation and behavior of Si-phonon during LHC the Si-phonons can be categorized as i) phonon frequencies in the range 495 - 510 cm⁻¹ (Lorentzian line shape) which are originating from the interface of Si NCs and SiO₂ matrix and ii) Phonon frequencies in the range 515 - 519 cm⁻¹ (asymmetric line shape) which are originating from core of Si NCs showing confinement effect on phonons. The important point to note is that blue shift of LF phonons is accompanied with the betterment in crystalline order taking it closer to crystalline Si phonon frequency. Stokes/anti-Stokes measurements show that LF phonons are observable due to Resonance enhancement of Raman signal. This understanding is also consistent with the observation of such a strong signal coming from interface of Si-SiO₂. Furthermore, our results of DFT/ TDDFT based Raman spectra calculations for Si₄₁ cluster with oxygen and hydrogen terminations establish the dominant contribution of interface phonon i.e. surface phonon with different terminations for smaller size Si.

Acknowledgment

It is a pleasure to acknowledge Dr. H. S. Rawat and Dr. G. S. Lodha for the continual support to this work. Ms Ekta Rani wishes to acknowledge help of Mr. Viresh Nayak in Matlab programming and Homi Bhabha National Institute, India for providing research fellowship during the course of this work. Authors also thank the scientific computing group of computer centre, RRCAT for the support in running the ADF code.

References

- ¹L. Pavesi, L. D. Negro, C. Mazzoleni, G. Franzo and F. Priolo, *Nature* **408**, 23 (2000).
- ²S. Kilpelaine, Y. W. Lu, F. Tuomisto, J. Slotte and L. A. Nylandsted, *arXiv.org* 1106.1173 [cond-matt.mat-sci] (2011).
- ³E. C. Cho, M. A. Green, G. Conibeer, D. Song, Y-H. Cho, G. Scardera, S. Huang, S. Park, X. J. Hao, Y. Huang, and L. V. Dao, *Advances in OptoElectronics* (2007).
- ⁴K. Seino, F. Bechstedt and P. Kroll, *Nanotechnology* **20**, 135702 (2009).
- ⁵L. V. Mercaldo, E. M. Esposito, P. D. Veneri, G. Fameli, S. Mirabella and G. Nicotra, *App. Phy. Let.* **97**, 153112 (2010).
- ⁶D. Song, E-C. Cho, G. Conibeer, Y. Huang, C. Flynn, M. A. Green, *J. of App. Phys.* **103**, 083544 (2008).
- ⁷M. Green, *Third Generation Photovoltaics: Advanced, Solar Energy, Conversion* Springer, Berlin (2003).
- ⁸I. F. Crowe, M. P. Halsall, H. Oksana, A. P. Knights, R. M. Gwilliam, M. Wojdak and A. J. Kenyon, *J. Appl. Phys.* **109**, 083534 (2011).
- ⁹G. H. Li, K. Ding, Y. Chen, H. X. Han and Z. P. Wang, *J. Appl. Phys.* **88**, 1439 (2000).
- ¹⁰A. N. Mikhaylov, A. I. Belov, A. B. Kostyuk, I. Yu. Zhavoronkov, D. S. Korolev, A. V. Nezhdanov, A. V. Ershov, D. V. Guseinov, T. A. Gracheva, N. D. Malygin, E. S. Demidov, D. I. Tetelbaum, *Physics of the Solid State* **54**, 2 368–82 (2012).
- ¹¹J. Bornacelli, J. Alejandro, R. Esqueda, L. R. Fernández and A. Oliver, *J. of Nanotechnology* 736478 (2013).
- ¹²O. L. Bratus, A. A. Evtukh, O. S. Lytvyn, M. V. Voitovych and V. O. Yukhymchuk, *Semiconductor Physics, Quantum Electronics & Optoelectronics* **14**, 2 247-55 (2011).
- ¹³C. Bonafos, et al. *J. Appl. Phys.* **95**, 5696 (2004).
- ¹⁴Y. Q. Wang, R. Smirani and G. G. Ross, *Nanotechnology* **15**, 1554–60 (2004).

- ¹⁵S. Guha, S. B. Qadri, R. G. Musket, M. A. Wall and T. S. Iwayama, *J. Appl. Phys.* **88**, 7 (2000).
- ¹⁶A. A. Sirenkoa, J. R. Foxa, I. A. Akimova, X. X.Xia, S. Ruvimovc and Z. L. Weber, *Solid State Communications* **113**, 553–58 (2000).
- ¹⁷G. Zatoryb, A. Podhorodecki, X. J. Hao, J. Misiewicz, Y. S. Shen and M. A. Green *Nanotechnology* **22**, 335703 (2011)
- ¹⁸T. Ye-Liao, Z. Yu-Hua, Z. Jun, X. Chun-Lai, C. Bu-Wen, W. Qi-Ming and X. J. Chin, *Phys. B* **21**, 7 077402 (2012)
- ¹⁹K. Ma, J. Y. Feng and Z. J. Zhang, *Nanotechnology* **17**, 4650–53 (2006)
- ²⁰C. Ternon, F. Gourbilleau, X. Portier, P. Voivenel and C. Dufour, *Thin Solid Films* **419**, 5–10 (2002).
- ²¹V. Paillard, P. Puech, M. A. Laguna, R. Carles, B. Kohn and F. Huisken, *J. Appl. Phys.* **86**, 1921 (1999).
- ²²G. Faraci, S. Gibilisco, P. Russo, A. R. Pennisi, G. Compagnini, S. Battiato, R. Puglisi and S. L. Rosa, *Eur. Phys. J. B* **46**, 457–61 (2005).
- ²³M. J. F. Zhou, F. Q. Song, C. R. Yin, M. D. Liu, J. G. Wan and G. H. Wang, *The European Physical Journal D - Atomic, Molecular, Optical and Plasma Physics* **24**, 1 269-72 (2003).
- ²⁴L. Wei-Long, J. Rui, L. Ming, C. Chen, X. Chang-Qing, Z. Chen-Xin, L. Hao-Feng, Z. Pei-Wen, Y. Tian-Chun, *Chin. Phys. Lett.* **26**, 4 046801 (2009).
- ²⁵I. Stenger, B. Gallas, B. Jusserand, S. Chenot, S. Fisson and J. Rivory, *Eur. Phys. J. Appl. Phys.* **44**, 51–57 (2008).
- ²⁶T. Arguirov, T. Mchedlidze, M. Kittler, R. Rölver, B. Berghoff, M. Först and B. Spangenberg, *App. Phys. Lett.* **89**, 053111 (2006)

- ²⁷C. M. Hessel, J. Wei, D. Reid, H. Fujii, M. C. Downer, and B. A. Korgel, *J. Phys. Chem. Lett.* **3**, 1089 (2012)
- ²⁸Y. Q. Wang, G. L. Kong, W. D. Chen, H. W. Diao, C. Y. Chen, S. B. Zhang and X. B. Liao, *App. Phys. Lett.* **81**, 22 (2002).
- ²⁹S. Hernández, P. Pellegrino, A. Martínez, Y. Lebour, B. Garrido, R. Spano, M. Cazzanelli, N. Daldosso, L. Pavesi, E. Jordana and J. M. Fedeli, *J. Appl. Phys.* **103**, 064309 (2008).
- ³⁰T. Okada, T. Iwaki, K. Yamamoto, H. Kasahara and K. Abe, *Solid State Communications* **49**, 8 809-912 (1984).
- ³¹T. N. Warang, D. Kabiraj, D. K. Avasthi, K. P. Jain, K. U. Joshi, A. M. Narsale and D. C. Kothari, *Surface & Coatings Technology* **203**, 2506–09 (2009).
- ³²H. S. Mavi, B. G. Rasheed, A. K. Shukla, S. C. Abbi and K. P. Jain, *J. Phys. D: Appl. Phys.* **34**, 292–98 (2001).
- ³³Md. N. Islam, A. Pradhan and S. Kumar, *J. Appl. Phys.* **98**, 024309 (2005).
- ³⁴E. Fazio, E. Barletta, F. Barreca, F. Neri and S. Trusso, *J. Vac. Sci. Technol. B* **23**, 519 (2005).
- ³⁵F. Fang, W. Zhang, J. Sun, N. Xu, J. Zhu, Z. Ying and J. Wu, *J. Mater. Res.* **24**, 7 (2009).
- ³⁶T. Seto, T. Orii, M. Hirasawa, N. Aya, *Thin Solid Films* **437**, 230–34 (2003).
- ³⁷J. R. Rani, V. P. Mahadevan, V. P. Pillai, R. S. Ajimsha, M. K. Jayaraj and R. S. Jayasree, *J. Appl. Phys.* **100**, 014302 (2006).
- ³⁸H. S. Mavi, S. Prusty, A.K. Shukla, S.C. Abbi *Thin Solid Films* **425**, 90–96 (2003).
- ³⁹A. Chaturvedi, M. P. Joshi, E. Rani, A. A. Ingale, A. K. Shrivastava and L. M. Kukreja, *J. of Luminescence* **154**, 178-184 (2014).
- ⁴⁰I. H. Campbell and P. M. Fauchet, *Solid State Comm.* **58**, 739 (1986).
- ⁴¹G. Dolling and R. A. Cowley, *Proc. Phys. Soc.* **88**, (1966).

- ⁴²P. Mishra and K. P. Jain, *Materials Science and Engineering B* **95**, (2002) & ref. therein.
- ⁴³P. Mishra and K. P. Jain, *Phys. Rev. B* **64**, 073304 (2001).
- ⁴⁴H. Kohno, T. Iwasaki, Y. Mita and S. Takeda, *J. Appl Phys.* **91**, 5 (2002).
- ⁴⁵J. Zi, *Phys. Rev. B* **55**, 15 (1997).
- ⁴⁶M. J. Konstantinovic', S. Bersier, X. Wang, M. Hayne, P. Lievens, R. E. Silverans and V. V. Moshchalkov, *Phy. Rev. B* **66**, 161311(R) (2002).
- ⁴⁷M. Zhixun, L. Xainbo, K. Guanglin, C. Junhao, *Science in China* **43**, 4 (2000).
- ⁴⁸S. K. Gupta, P. K. Jha, *Solid State Communications* **149**, 1989-92 (2009) and ref. therein.
- ⁴⁹S. K. Arguirova, Tz. Arguirov, D. Wolfframm and J. Reif, *J. Appl. Phys.* **94**, 8 (2003).
- ⁵⁰Y. Duan Y, J. F. Kong, W. Z. Shen, *J. of Raman Spectroscopy* DOI 10.1002/jrs.3094 (2011).
- ⁵¹E. Rani, A. A. Ingale, A. Chaturvedi M. P. Joshi and L. M. Kukreja (To be submitted).
- ⁵²M. Molinari, H. Rinnert and M. Vergnat, *Appl. Phys. Lett.* **77**, 3499 (2000).
- ⁵³E. Rani, A. Ingale, A. Chaturvedi, M. P. Joshi and L. M. Kukreja (To be submitted)
- ⁵⁴G. Hadjisavvas and P. C. Kelires, *Phys. Rev. Letts.* **93**, 226104 (2004).
- ⁵⁵M. Ippolito, S. Meloni and L. Colombo, *App. Phys. Lett.* **93**, 153109 (2008).
- ⁵⁶S. Kim, M. C. Kim, S. H. Choi, K. J. Kim, H. N. Hwang and C. C. Hwang, *Appl. Phys. Lett.* **91**, 103113 (2007).
- ⁵⁷D. E. Yilmaz, C. Bulutay and T. Cagin, *Physical Review B* **77**, 155306 (2008).
- ⁵⁸D. E. Yilmaz, "Thesis: On the strain in Silicon nanocrystals" Bilkent University Turkey (2009).
- ⁵⁹M. Roussel, E. Talbot, P. Pareige and F. Gourbilleau, *J. Appl. Phys.* **113**, 063519 (2013).
- ⁶⁰G. Lucovsky, A. Banerjee, B. Hinds, B. Claflin, K. Koh, H. Yang, *J. Vac. Sci. Technol. B* **15**, 4 (1997) & references therein.

- ⁶¹D. Chrobak, N. Tymiak, A. Beaver, O. Ugurlu, W. W. Gerberich and R. Nowak, *Nature Nanotechnology* **6**, (2011).
- ⁶²C. L. Rountree, D. Vandembroucq, M. Talamali, E. Bouchaud and C. Roux, *Phys. Rev. Lett.* **102**, (2009).
- ⁶³T. R. Hart, R. L. Aggarwal and B. Lax, *Phys. Rev. B* **1**, 2 (1970)
- ⁶⁴G. Faraci, S. Gibilisco and A. R. Pennisi, *Phys. Rev. B* **80**, 193410 (2009).
- ⁶⁵P. Hohenberg and W. Kohn, *Phys. Rev.*, **136**, B864 (1964); W. Kohn and L. J. Sham, *ibid.* **140**, A1133 (1965)
- ⁶⁶E. J. Baerends, J. Autschbach, A. Berces, et al. *Amsterdam Density Functional, Theoretical Chemistry*, Vrije Universiteit, Amsterdam, URL <http://www.scm.com>; J. P. Perdew, K. Burke, and M. Ernzerhof, *Phys. Rev. Lett.*, **77**, 3865 (1996).
- ⁶⁸H. Xia, Y. L. Wang, W. Zang, X. N. Liu, X. K. Zhang and D. Fang, *J. Appl. Phys.* **78**, 11 (1995).
- ⁶⁹J.-H. Shima, S. Imb, N. -H. Choa, *Applied Surface Science* **234** 268–273(2004).
- ⁷⁰M. F. Cerqueira, T.V. Semikina, N. V. Baidus, E. Alves, *Int. J. Materials and Product Technology*, **39**, 1/2, 195-204 (2010).
- ⁷¹X. L. Wu, G. G. Siu, S. Tong, X. N. Liu, F. Yan, S. S. Jiang, X. K. Zhang, and D. Feng, *Appl. Phys. Lett.* **69**, 4 (1996).

